Journal of Combinatorial Mathematics
and Combinatorial Computing
www.combinatorialpress.com/jcmcc

Combinatorial Press

Study on the effect of asphalt pretreatment on the structural and electrochemical properties of porous carbon based on finite element analysis

Haocheng Xiong[1,✉], Haowen Zheng[1]

[1] *School of Civil and Resources Engineering, University of Science and Technology, Beijing, 100083, China*

ABSTRACT

Bitumen is a high-quality raw material for the preparation of carbon materials due to its high carbon and low ash characteristics, and its use in the preparation of supercapacitor electrode materials plays a significant role in the enhancement of the economic benefits of the entire coal chemical process. In this paper, the raw materials and experimental equipment required for this study were selected to prepare porous carbon samples under the guidance of the raw material pretreatment process. After completing the preparation of porous carbon samples, the finite element analysis software ANSYS was used to investigate the effect of bitumen pretreatment on the structure and electrochemical properties of porous carbon. With the rising air oxidation time, the peak ratio of porous carbon showed a trend of decreasing and then increasing, with specific values of 2.627, 1.958, 2.083, and 2.486, which was the same trend as that of the XRD test results, suggesting that the asphalt pretreatment has a moderating effect on the structure of porous carbon. The study in this paper further recognizes the effect of asphalt pretreatment on the structure and electrochemical properties of porous carbon, which provides a reference for research and development and innovation in materials chemistry.

Keywords: finite element analysis, asphalt pretreatment, porous carbon, electrochemical properties

1. Introduction

The rapid increase of greenhouse gas concentration in the atmosphere has caused serious negative impacts on the ecological environment, and renewable energy has been rapidly developed and popularized in the context of "carbon peaking and carbon neutrality" [1-2]. The construction of electric vehicle industry and smart grid makes energy storage technology become the key link of energy redistribution. Electrochemical energy storage, as an important part of the energy storage system, is a device that utilizes chemical reactions to directly convert electrical energy [3]. The electrode material determines the energy density and electrochemical characteristics of the battery and is a key

✉ Corresponding author.
E-mail address: 13071130135@163.com (H. Xiong).
Received 10 January 2024; Revised 15 March 2024; Accepted 25 December 2024; Published Online 16 April 2025.
DOI: 10.61091/jcmcc127b-374

component in energy storage devices [4]. Porous carbon materials with rich pore structure have the natural advantages of good electrical conductivity, stable structure, abundant resources, and low price, which can be used directly as electrode materials to construct carbon-based electrochemical energy storage devices, and can be compounded with non-carbon electroactive materials to play the roles of transporting electrons, buffering the volume expansion, and regulating the interfacial reaction, and have been playing an indispensable role in energy storage devices [5-8]. When porous carbon materials are used as energy storage materials, good electrical conductivity, suitable surface chemistry, large specific surface area and porosity are the key factors to improve the storage capacity and stability of energy storage devices. Structural design and functionalization of porous carbon materials can cause changes in the physical and chemical properties of porous carbon materials [9]. In addition, the orderliness of the pore structure and the closure of the pores have a significant effect on the electrochemical properties of porous carbon materials [10]. However, porous carbon materials (called activated carbon in the industry) are currently industrially obtained mainly by carbonization and activation of raw materials such as petroleum coke, coal-based, plant-based or polymer resins, which makes it difficult to achieve precise modulation of the product structure due to the uncertainties in the raw material sources and structures, affecting the electrochemical performances of carbon materials [11-13]. The biggest challenge facing the preparation and structure modulation of carbon electrode materials is to find one or more outstanding advantages according to the application requirements, while taking into account the comprehensive performance of other aspects [14-15]. Therefore, various constraints in porous carbon materials need to be harmonized by rationally designing their porous structures. Researchers are committed to the development of novel synthetic methods for the preparation of porous carbon materials with novel structures to facilitate the reaction kinetics and enable the materials to have superior electrochemical properties.

With the development of new material science, environmental protection technology, fine chemicals, and asphalt engineering technology, asphalt pretreatment techniques are becoming more and more diversified, such as desalination, dehydration, and decontamination carried out by oxidative cross-linking, emulsification, and catalytic techniques [16-18]. Under the current application of these technologies, the structure and electrochemical properties of porous carbon materials can be significantly improved, but there are still three major pain points, which are the ambiguity of the relationship between structural parameters and performance parameters, the escalation of the difficulty in observing the evolution process of the material structure under complex environments, and the observation of multiple technology models only for a single material [19-21]. It is evident that the necessity of exploring new asphalt pretreatment techniques for analyzing the structural and electrochemical properties of porous carbon. While finite element analysis, which uses mathematical approximation to simulate the real physical system (geometry and loading conditions) and can approximate the real system with infinite unknowns by a finite number of unknowns, has been widely used in nonlinear analysis of reinforced concrete structures and can be an advantageous method to study the structural and electrochemical properties of porous charcoal [22].

Before starting the research experiments, it is necessary to select the main raw materials and experimental apparatus for this research, and prepare the porous carbon samples, which are CNAC-1h, CNAC-1.5h, CNAC-2h, CNAC-2.5h, in combination with the corresponding means of raw material pretreatment. In order to show the effect of asphalt pretreatment on the structural and electrochemical properties of the porous carbon more clearly, the FEA framework to study the structure and electrochemical properties of porous carbon. According to the operation principle and steps of this program, the effects of asphalt pretreatment on the structural and electrochemical properties of porous carbon were investigated, aiming at revealing the interaction mechanism between the two.

2. Experimental section

This chapter focuses on determining the experimental raw materials, pretreatment process (although thermal polymerization method and air oxidation method are introduced, while air oxidation method is mainly used in this paper), after which the preparation of porous charcoal samples for this research is started to provide solid theoretical support for the following research work to be carried out. The detailed principle is as follows:

2.1. Raw materials

In this experiment, coal asphalt was used as raw material, and its characteristic parameters were: TI 30.05%, volatile matter 52.22%, softening point 83℃. Elemental analysis: C 92.3%, H4-16%, S0.42%, 0+N3.12%.

2.2. Raw material pretreatment process

2.2.1. Thermal polymerization methods. The coal pitch was put into a crucible with a lid and moved into a box-type resistance furnace at room temperature, which was rapidly heated up to 450℃, with constant temperature ranging from 3h~6h and 8h~13h, respectively.

2.2.2. Air oxidation. The air oxidation was carried out by the tube furnace programmed heating method, which was ramped up to 420°C for 1h, 1.5h, 2h, and 2.5h, respectively, and then kept at a constant temperature for 3h.

2.3. Preparation of porous carbon materials

Porous carbon preparation process: the raw material coal asphalt was fully ground in an agate mortar, the powdered coal asphalt was spread in a porcelain boat and put into a tube furnace, heated in air at a rate of 8 ℃/min to 800 ℃ and heated at a constant temperature for 4 h. After cooling down to room temperature and taking out the sample in the boat, the pre-oxidized coal asphalt powder was obtained by grinding the sample fully. First of all, take 2g of pre-oxidized bitumen, 1 g of calcium carbonate nanometer, 2g of sodium chloride (mass ratio of 2:1:2) in the agate mortar grinding evenly in the porcelain boat and placed in a tube furnace in nitrogen at a rate of 8 ° C / min heating rate of 800 ° C and holding time of 6h. To be cooled to room temperature and then remove the porcelain boat will be fully ground in the 120 ° C water bath water wash for 4h, and then acid wash for 6h and Filtering, and finally washed to neutral, the product was dried at constant temperature 28 to obtain CNC. The dried sample CNC and KOH were mixed and ground in the mass ratio of 2:4, then spread in the porcelain boat and put into the tube furnace for activation with a good lid, and then heated up to 800 ℃ under nitrogen atmosphere at the rate of 88 ℃/min, and kept warm for 4 h. After cooled down to room temperature, the boat was removed from the porcelain boat, and then fully ground, and then acid washed at 80 ℃ in a water bath for 6 h, and then pumped and filtered, and then dried the product for 24 h. The black solid powder obtained was CNAC-1h, which was named CNAC-1h. The black solid powder obtained was coal pitch-based porous carbon, and the sample was named CNAC-1h. For comparison, the samples were prepared and named as CNAC-1.5h, CNAC-2h, CNAC-2.5h by changing the oxidation time under the same other preparation conditions (1.5h, 2h, 2.5h). Meanwhile, CNC and KOH were fully milled in an agate mortar in the mass ratio of 1:3. The mixed samples were put into a horizontal tube furnace for chemical activation and heated up to 900 °C at a rate of 2.3 °C/min under nitrogen atmosphere and held for 4 h. The porous carbon samples, CNAC, were obtained after water and acid washing.

2.4. Preparation and assembly of porous carbon electrode materials

The chemical tests were carried out in a three-electrode system, and the asphalt-based porous carbon electrodes were prepared as follows: nickel foam was cut into 2 cm × 3.0 cm size, ultrasonically cleaned and then dried at a constant temperature of 80°C for 2 h for spare parts, and the mass of the nickel foam was weighed and recorded prior to use, M1. The experimentally prepared asphalt-based porous carbon materials, CNAC-600~CNAC900, were mixed with these four asphalt-based porous carbon materials As the active material, PTFE emulsion and acetylene black were mixed in the mass ratio of 6:2:2, fully milled for 45 min to paste and uniformly coated on the (2cm×3cm×2.0mm) Ni foam collector, and dried at a constant temperature of 65°C for 12 h. The dried electrodes were pressed to obtain working electrodes, and the mass of coated electrodes was weighed (M2), and the mass of the active material was calculated (M2-M1), to ensure the uniformity of each piece of electrode.), in order to ensure the uniformity of each piece of electrode, the mass of the active substance was kept at about 4 mg. The long strip of nickel foam coated with Hg/HgO electrode and platinum sheet electrode in 6 MKOH solution was formed into a three-electrode system. Two pieces of NCPHC-1000 nickel foam coated with the same mass were separated by a diaphragm, dropwise added with 6MKOH solution, and encapsulated in a button cell case to form a two-electrode battery device for electrochemical performance testing.

3. Structural and electrochemical properties of porous carbon in the framework of finite element analysis

With the theoretical support of Chapter 2, the preparation of porous carbon samples was completed. In order to more intuitively observe the effect of asphalt pretreatment on the structural and electrochemical properties of porous carbon, a research program on the structural and electrochemical properties of porous carbon in the framework of finite element analysis was developed with the support of finite element simulation and analysis software. The main contents of this chapter are as follows:

3.1. Finite element simulation analysis

3.1.1. Principles of Finite Element Analysis. Most of the laws of physics are spatio-temporal related problems and are usually expressed mathematically using partial differential equations (PDEs). In many research problems, it is extremely difficult to solve the analytical solutions of PDEs when very complex geometries are considered, but it is possible to derive the corresponding numerical model equations by making discrete approximations to the PDEs, and the approximate solutions of PDEs can be obtained by solving the numerical model equations. The finite element method (FEM) is used to compute these approximate solutions, and is an indispensable part of engineering analysis to provide a more accurate view of predictable phenomena in complex real-world problems [23]. The advantages of FEM in various research fields are obvious to all, and the visualization and analysis of the physical processes through computers can make the design more reliable, safe, and cost-effective, so the FEM has been widely used in various fields. Therefore, the finite element method (FEM) is found in various industries. Today, FEM may be used to analyze every important engineering design and in every branch of scientific research. The finite element method is now mainly used through the application of commercial finite element programs. These programs are often installed in mainframe computers, workstations and personal computers and are used to solve very complex problems. While FEM was originally used to analyze solids and structures, it is now also used to analyze problems including fluid mechanics, structural mechanics, and multi-physics field problems.

Traditionally, finite element analysis (FEA) is mainly based on structural mechanics modeling, and only to a lesser extent on heat transfer. With the increasing application of multiphysics field modeling,

the finite element method has been commonly used in fluid flow and electromagnetic simulation, and the term “finite element analysis” has gradually been accepted and recognized in other engineering and scientific fields. In fact, the finite element analysis process is the same regardless of the application area. The first step is to “tighten” the geometry model. In order to prepare a geometry for FEA, it is often necessary to repair and remove features from the geometry. Repair operations repair the parts of the geometry that are not “tightly connected”, while feature removal operations remove elongated surfaces or merge small redundant edges. Next, material properties and material property functions need to be defined and assigned. The ontological relationships in the mathematical model involve physical properties of the material that may be related to the modeling variables (dependent variables). For example, in thermal expansion analysis, mechanical and thermal properties are often temperature dependent. Afterwards equations, loads or constraints are assigned to entities such as geometric domains, boundaries, edges and points, after which a complete numerical model can be obtained by creating a mesh, the above related definitions are part of the pre-processing process in finite elements. Finally the solution of the equations is obtained under the specified study.

3.1.2. Overview of Finite Element Analysis Software. With the rapid advancement of technology and computers, the prevalence of the finite element method has permeated almost all technological fields.Finite element software is a computer program used to solve problems using the finite element method. Finite element software is used to create numerical models of physical systems, which are then solved using the finite element method. The software can be used to analyze a wide range of problems, from simple static problems to complex dynamic problems. Finite element software is frequently used in many industries such as aerospace, automotive, civil engineering and manufacturing, etc. Some of the more popular finite element software packages include ANSYS, ABAQUS, COMSOL Multiphysics, and ABSQUS, etc., while this paper adopts the ANSYS software. ANSYS software focuses on the expansion of application areas, and currently covers the flow of structural mechanics, fluid dynamics, heat conduction and heat transfer. , fluid dynamics, heat transfer and electromagnetism and other very broad research areas [24]. It has a good reputation among users dedicated to linear analysis, and it has also made a large contribution to the utilization of computer resources and the development of user interfaces.

3.2. Material characterization

3.2.1. XRD characterization. X-ray diffraction analysis is mainly used to characterize the structure and defects of crystalline materials, but also qualitatively characterize non-crystalline materials [25]. In this paper, XRD characterization of MCC and NSMCC series materials was carried out using an X-ray diffractometer (D8ADVAHCL type) under the test conditions of radiation source of Ka Cu target, λ of 0.154 nm, tube current of 30 mA, tube voltage of 40 KV, and scanning angle of 20 of 10-90 °, respectively, and R-value of the materials and layer spacing were calculated. The equations are shown below:

$$R = H_1 / H_2 \tag{1}$$

Where: H_1 and H_2 are shown in Fig. 1, respectively, the value of R can characterize the degree of disorder of the material, and the smaller the value of R, the more disordered represents the carbon material.

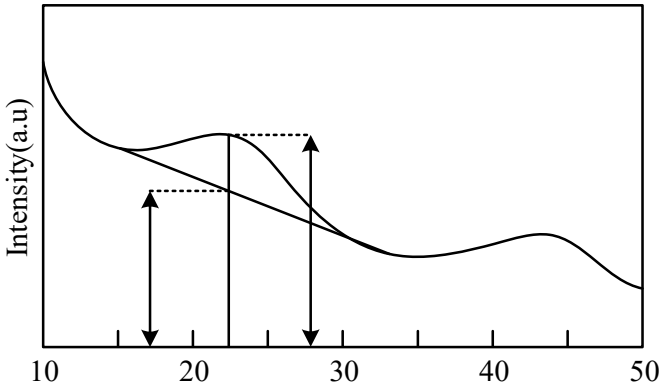

Fig. 1. Schematic diagram of r value calculation formula

The formula for calculating the material layer spacing is as follows:

$$2d\sin\theta = n\lambda \tag{2}$$

Where: d is the crystallographic distance of the material, 0 is the radian corresponding to the peak position, n is the wavelength of the ray (a positive number), and λ = 0.15406 nm (Cu target Ka ray).

3.2.2. Raman spectroscopy. Raman spectroscopy can be used to qualitatively analyze the chemical structure and crystallinity of materials, and can also be used to probe the defects and graphitization of carbon materials. In this paper, Raman characterization of MCC and NSMCC series materials was carried out using a laser Raman spectrometer (HR800 model) under the test condition of laser wavelength of 532 nm, and the degree of disorder of different materials was obtained by calculation.

3.2.3. Specific surface area and pore size distribution of materials. Nitrogen physical adsorption and desorption tests are based on Brunner-Emmet-Teller theory and density functional theory (DFT) to detect some physical and chemical properties of materials. In this paper, PSAC, MCC and NSMCC series of materials were characterized using an IQ2 instrument manufactured by Kantar Corporation, USA, and parameters such as specific surface area as well as pore size distribution of different materials were obtained.

3.2.4. Scanning electron microscopy. Scanning electron microscopy can be used to analyze the material surface structure and elemental distribution, etc. In this paper, PSAC, MCC and NSMCC series materials were characterized using a field emission scanning electron microscope (ZEISS IGMA/HD type), and the microscopic morphology as well as the elemental distribution of the materials were obtained.

3.2.5. XPS testing. X-ray photoelectron spectroscopy (XPS) can be used to analyze the elemental compositions and valence states on the surface of a material through the bonding states. In this paper, MCC and NSMCC series materials were characterized using an XPS instrument (Axis Ultra DLD model) to obtain the elemental species and contents on the surface of the materials, respectively.

3.3. Electrochemical performance testing

3.3.1. Constant current charging and discharging. In this paper, constant-current charge/discharge tests were carried out on symmetrical snap supercapacitors by an electrochemical workstation (CHI660E), with an operating voltage range of 0-1 V. Constant-current charge/discharge tests were carried out on sodium-ion half-batteries and sodium-ion capacitors by using a battery test system (CT300IA), with test voltages ranging from 0.01-3 V (based on copper foil vs. Na/Na^+), 2.5-4.2V (based on aluminum foil vs. Na/Na^+), and 0-4V (for the sodium-ion capacitor). And the specific

capacity, energy density and power density of the energy storage device were calculated based on constant current charging and discharging. The formulas are shown below:

1) Supercapacitor:

(1) Mass specific capacity:

$$C_g = 2 \times I \times t / (m \times \Delta U) \tag{3}$$

Where: C_g is the mass specific capacity of a single electrode (Fg^{-1}), I is the discharge current (A), t is the discharge time (s), m is the mass of the active substance on a single electrode (g), and AU is the voltage drop corresponding to the discharge time (V).

(2) Area specific capacity:

$$C_a = C_g \times m_1 \tag{4}$$

Where: C_a is the area specific capacity of a single electrode (F/cm^2). C_g is the mass specific capacity of a single electrode (Fg^{-1}). m_1 is the mass of a single electrode ($mg\,cm^2$).

(3) Area normalized capacitance:

$$C_s = C_g / S_{BET} \tag{5}$$

Where: C_s is the area-normalized capacitance of a single electrode (μFcm^2). S_{RET} is the specific surface area of the electrode material (m^2g^{-1}).

(4) Energy density:

$$E = C_g \times V^2 / (2 \times 4 \times 3.6) \tag{6}$$

Where: E is the energy density of the supercapacitor ($Wh\,kg^{-1}$\), Cg is the mass specific capacity of the individual electrodes (Fg^{-1}), and V is the voltage of the test window of the supercapacitor.

(5) Power density:

$$P = 3600 \times E / t \tag{7}$$

Where: P is the super power density (Wkg^{-1}), E is the energy density of the supercapacitor ($Wh\,kg^{-1}$), and t is the discharge time.

2) Calculation formula for sodium-ion half-cells and sodium-ion capacitors:

(1) Mass ratio capacitance:

$$C = I / [(dE / dt \times m)] \approx I / [(\Delta E / \Delta t \times m)] \tag{8}$$

Where C is the mass specific capacitance, (Fg^{-1}) is the constant current charge/discharge current (A), Δt is the discharge time (t). ΔE is the voltage drop corresponding to the discharge time (V), and m is the total mass of the active substance of the electrode material (g).

(2) Energy density:

$$E = CU^2 / (2 \times 3.6) \tag{9}$$

Where: E is the energy density ($Wh\,kg^{-1}$), C is the mass specific capacitance (Fg^{-1}), and U is the test window voltage (V) of the sodium ion capacitor.

(3) Power density:

$$P = 3600 \times E / t \tag{10}$$

Where P is the power density (Wkg^{-1}), and t is the discharge time (s) of the sodium ion capacitor.

3.3.2. Cyclic voltammetry. In this paper, constant-current charge/discharge tests for determining the redox potential, capacitance, and diffusion behavior of the materials were performed on symmetrical snap supercapacitors, sodium-ion half-cells, and sodium-ion capacitors by means of electrochemical workstations (CHI660E) with test voltages ranging from 0-IV (for supercapacitors), 0.01-3V (based on

Cu-foil vs. $NaNa^+$), 2.5-4.2V (based on Al-foil vs. $NaNa^+$) and 0-4V (sodium ion capacitors). In addition, the b-value, surface capacitance share and diffusion coefficient D of the materials were calculated based on the CV curve data, respectively, and the equations are shown below:

1) b-value. The b-value is a performance indicator of the percentage of capacitance effect of the material, when the b-value is between 0.5-0.75 the material is considered to be a diffusion-controlled process, and b is close to 1. 0 corresponds to a surface capacitance-dominated process. That is:

$$i = av^b \tag{11}$$

Where i is the current intensity and v is the scan rate.

2) Surface capacitance percentage:

$$I(V) = k_1 v + k_2 v^{\frac{1}{2}} \tag{12}$$

where $I(V), k_1 v$ and $k_2 v^{\frac{1}{2}}$ represent, respectively, the total current at a given voltage, the current generated by the surface capacitance, and the current generated by the diffusion-controlled Na^+ embedded generated current.

3) Diffusion coefficient D. Sodium ion diffusion coefficient D is an index to characterize the good or bad diffusion performance of the material, and the larger its value represents the better its diffusion performance. Namely:

$$D = \frac{4}{\pi\tau} \frac{m_B V_m}{M_B A}^2 \frac{\Delta E_s}{\tau(dE\tau / d\sqrt{\tau})}^2 \tag{13}$$

where τ is the pulse time (in s), ΔE_s represents the voltage change when the voltage reaches the steady state, m_B is the mass of the active substance, M_B is the molar mass of the electrode material, V_m is the molar volume, and A is the electrode surface area. When the voltage is linearly correlated with $\tau^{1/2}$, the formula can be further simplified to Eq. (ΔE_τ is the potential change of the constant-current pulse after removing the voltage drop, and the rest of the parameters are the same as in Eq.):

$$D = \frac{4}{\pi\tau} \frac{m_B V_m}{M_B A}^2 \frac{\Delta E_s}{\Delta E_\tau}^2 \tag{14}$$

3.3.3. AC impedance. In this paper, AC impedance tests were performed on symmetrical snap supercapacitors, sodium-ion half-cells and sodium-ion capacitors respectively by electrochemical workstation under the test conditions of amplitude of 5 mV and frequency of 10°2Hz-10°Hz, and used with the speculative equivalent circuit diagram to calculate the solid electrolyte interface membrane (SEI membrane) impedance, charge transfer impedance, and ionic diffusion coefficient parameters. The equations are shown below:

$$Z' = R_3 + R_S + \sigma\omega^{-\frac{1}{2}} \tag{15}$$

where R_3 is the charge transfer impedance, R_s is the internal resistance of the test cell, Ω is the angular frequency, and σ is the Warburg coefficient with respect to Z'. The Warburg coefficient σ is an indicator that characterizes how good a material's dynamics are, with smaller values indicating better ion diffusion.

4. Exploratory Analysis of Porous Carbon Structure and Electrochemical Properties

Under the theoretical guidance of the previous research program, finite element analysis software was used to investigate the role of asphalt pretreatment (air oxidation method) on the structural and

electrochemical properties of porous carbon samples. The effect of asphalt pretreatment on the structure of porous carbon samples is reflected in XPS, XRD material structure, Raman spectroscopy, material specific surface, and pore size distribution, while the interaction between asphalt pretreatment and the chemical properties of porous carbon samples is manifested in the three dimensions of constant-current charging and discharging, cyclic voltammetry, and AC impedance. The results and process of analyzing the specific experimental investigations in this chapter are as follows:

4.1. Effect of asphalt pretreatment on the structure of porous charcoal

Within the scope of asphalt pretreatment technology, the time of air oxidation method has a crucial influence on the structure, morphology and of the final prepared material, therefore, samples with different air oxidation times under the same activation conditions were characterized and analyzed in this regard. Considering the reason that the image under the scanning electron microscope is not clear, it will not be considered in the following. In this subsection, with the support of the finite element analysis software, we will investigate the effect of air oxidation method on the structure of porous carbon in asphalt pretreatment from four aspects, namely, XRD characterization, Raman spectroscopy, specific surface area and pore size distribution of the material, and XPS test. The specific analysis process is as follows:

4.1.1. XPS test analysis. In order to analyze the existence of oxygen atoms in the material after air oxidation, XPS test was carried out on the samples, and the test results are shown in Fig. 2. As shown in Fig. 2 (a) the XPS full spectrum of this series of samples, the oxygen content of the activated samples increased gradually with the increase of the oxidation time, but when the oxidation time reaches 2.5h, the oxygen content decreases, which may be due to the fact that the oxygen content of the samples is more than the other samples, which were shed in the form of CO2, CO, H2O, etc., in the process of activation. The oxygen content of the samples with oxidation time of 1, 1.5, 2, and 2.5h was 4.43, 7.27, 10.28, and 9.42%, respectively. As shown in Fig. 2(b-e) after fitting the O1s fine spectral splitting peaks, it can be seen that the oxygen atoms in the samples are mainly in the form of single-bonded oxygen, which indicates that the reaction that occurs in the asphalt molecule during the air oxidation is mainly the cross-linking between the planar aromatics as shown in Fig. 2(f) to become a more complex three-dimensional structure, and part of it is retained in the activation process.

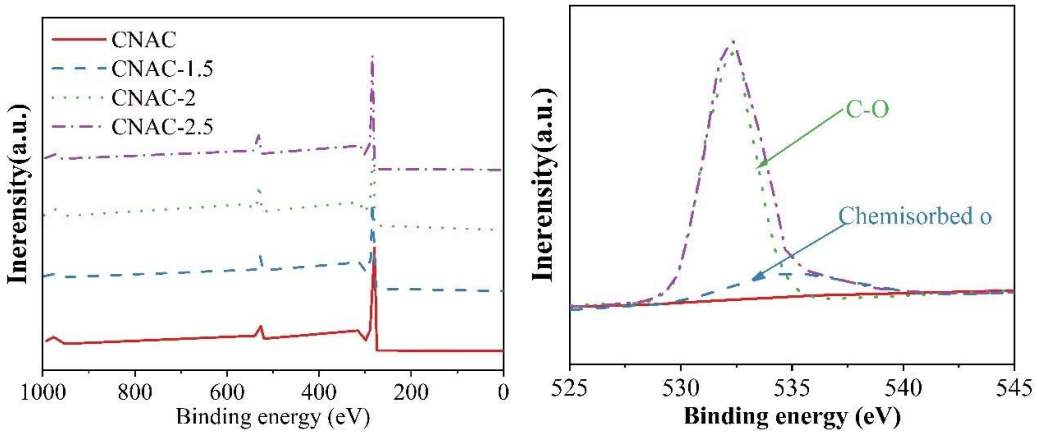

(a)XPS full spectrum (b)1h

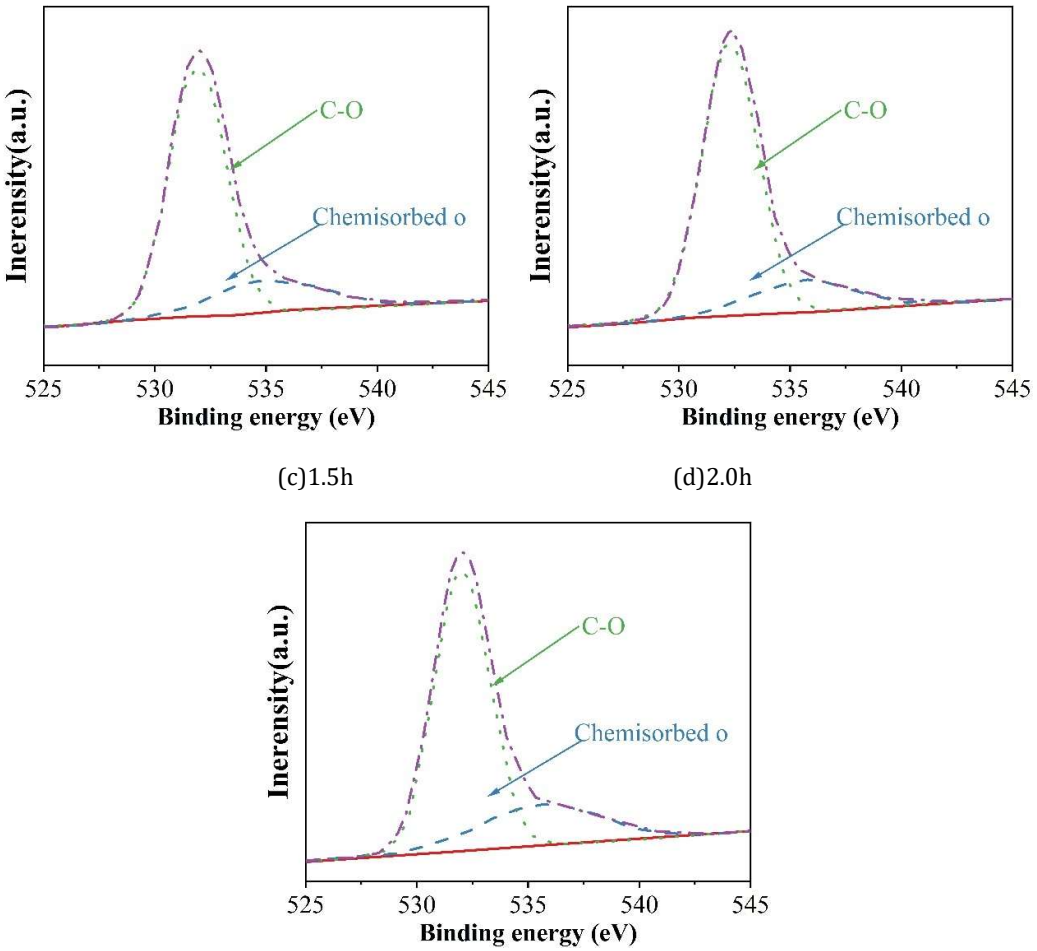

(c)1.5h (d)2.0h

(e)2.5h

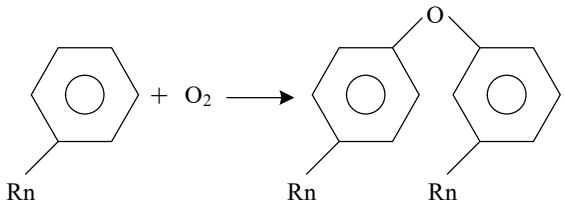

(f)Reaction equation

Fig. 2. XPS test analysis

4.1.2. XRD material structure characterization tests. In order to investigate the variation of physical composition and graphitization of the samples with air oxidation time, the materials were tested by XRD and fitted with split peaks, and the results are shown in Fig. 3, where (a) to (e) are XRD, 1h, 1.5h, 2h, and 2.5h, respectively. The samples were all highly disordered with broad peaks. The layer spacing of the samples decreases and then increases with increasing oxidation time. With the process of air oxidation, intermolecular cross-linking of thick cyclic aromatic hydrocarbons occurs, which promotes the transition from ordered carbon to disordered carbon. In this process, the presence of potassium hydroxide and its pore-making effect make a large number of micropores below 0.9 nm, which greatly affects the graphitization degree of the material, and at the same time, it is difficult to transform the thick cyclic structure cross-linked by oxygen atoms to graphitic carbon in the process of heat treatment,

and it is difficult to graphitize microcrystalline edges with more exposed sites are inclined to react with K2O and K2CO3 to generate gases escaping. When the oxidation time is short, the presence of a large number of ether bonds makes the thermal stability of the material increase, and the reactivity with potassium hydroxide decreases, while the oxidation time increases, the ether bond content does not increase significantly and the samples are difficult to form a graphite lamellar structure in the carbonization process, the edge of the active site, which is more likely to react with potassium hydroxide, and the interactions of these complex processes produce such a result.

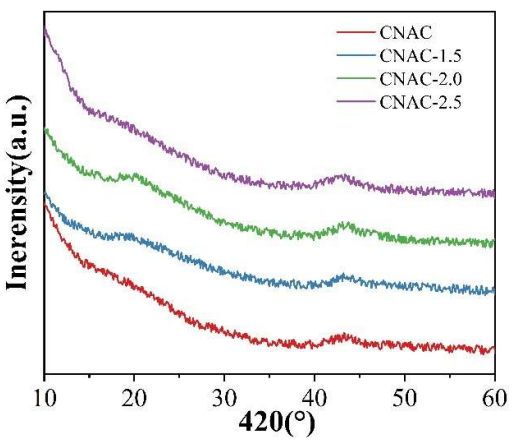

(a)XRD

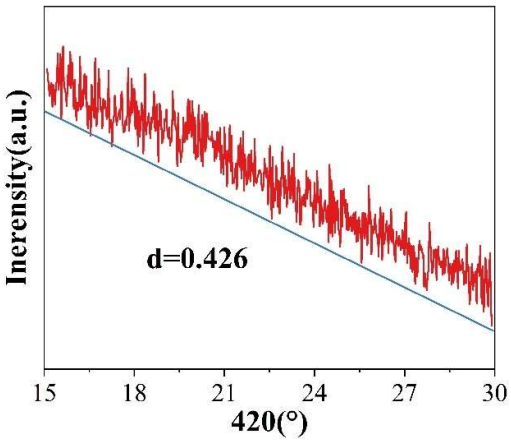

(b)1h

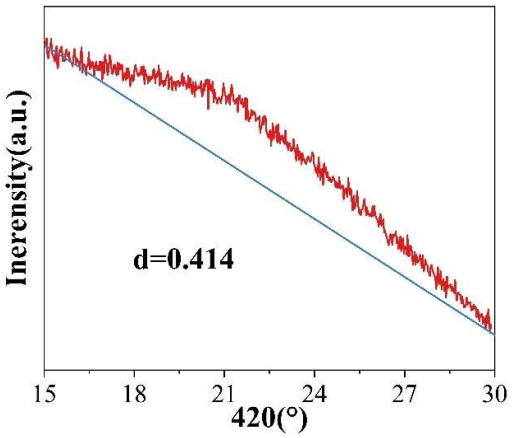

(c)1.5h

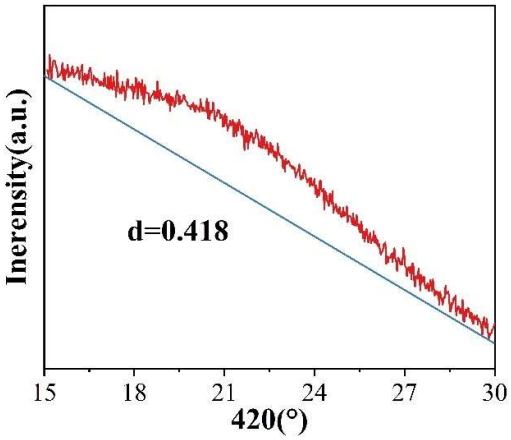

(d)2h

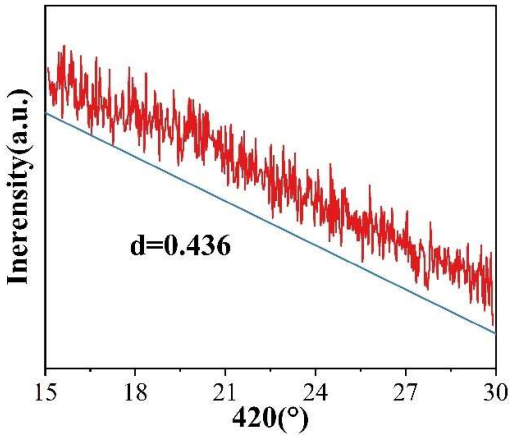

(e)2.5h

Fig. 3. XRD material structure characterization test

4.1.3. Raman spectroscopy test analysis. In order to further investigate the changes of the physical structure of the material with the air oxidation time, the material was again tested by Raman spectroscopy, and the test results are shown in Fig. 4, where (a) ~ (f) are the Raman spectra, 1h, 1.5h, 2h, 2.5h, and the peak ratio, respectively. As shown in the Raman test spectra of the samples in Fig. 4(a), the area of the D peak of the samples with different air oxidation times is larger than that of the G peak, which is the same as that of the XRD results, and proves that there are more defects present. After the split-peak fitting of the three is shown in Fig. 4(b-d), their Raman profiles can be fitted into four peaks, and the areas of their two main peaks, such as those shown in Fig. 4(e), also show the trend of decreasing and then increasing, which are 2.627, 1.958, 2.083, and 2.486 respectively, which are in line with the trend of changing the average layer spacing of the XRD test.

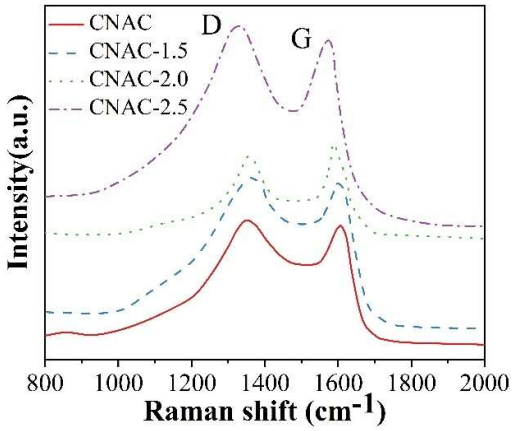

(a)Raman test map

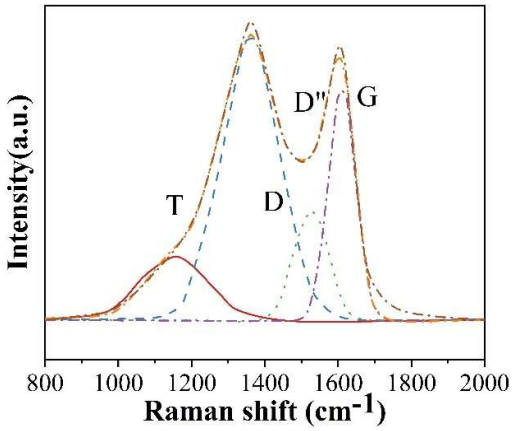

(b)1h

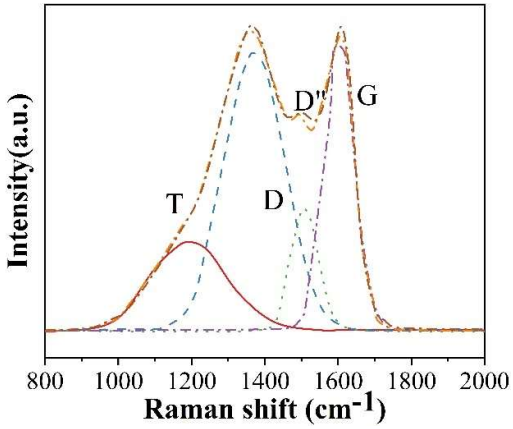

(c)1.5h

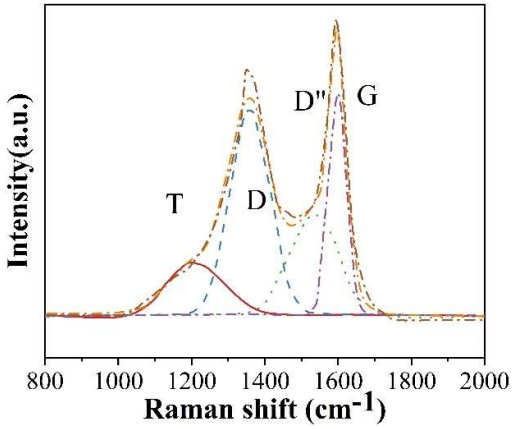

(d)2h

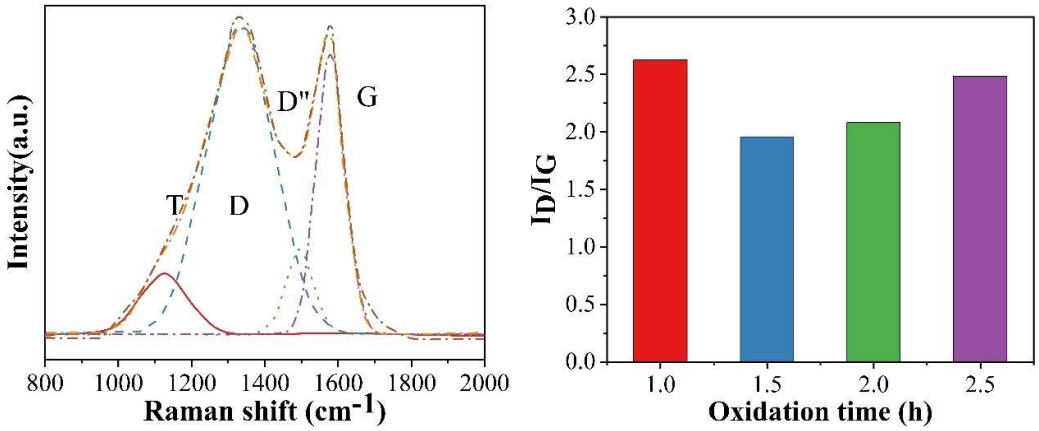

(e)2.5h (f)The ratio of peak D to peak G

Fig. 4. Raman spectrum test analysis.

4.1.4. Specific surface area and pore size distribution studies of materials. In order to investigate the effect of air oxidation time on the pore structure and specific surface area of the materials, nitrogen adsorption and desorption tests were carried out, and the test results are shown in Fig. 5, in which (a) to (c) are the nitrogen adsorption and desorption test curves, pore size distributions, and 0-10 nm pore size distributions, respectively, and the data of their pore structures are shown in Table 1. As shown in Fig. 5(a), the nitrogen adsorption and desorption curves of the materials show that the curves of all samples are characterized by type I isotherms. In Fig. 5(c), it can be clearly seen that the pore sizes of all materials are mainly distributed in the region to 0-2 nm, and the number of micropores in the material gradually increases with the increase of air oxidation time, and when the oxidation time increases to 2.5 h, the micropore content below 0.9 nm decreases and the micropores above 0.9 nm increase significantly, so the specific surface area of the sample also increases with the increase of oxidation time.

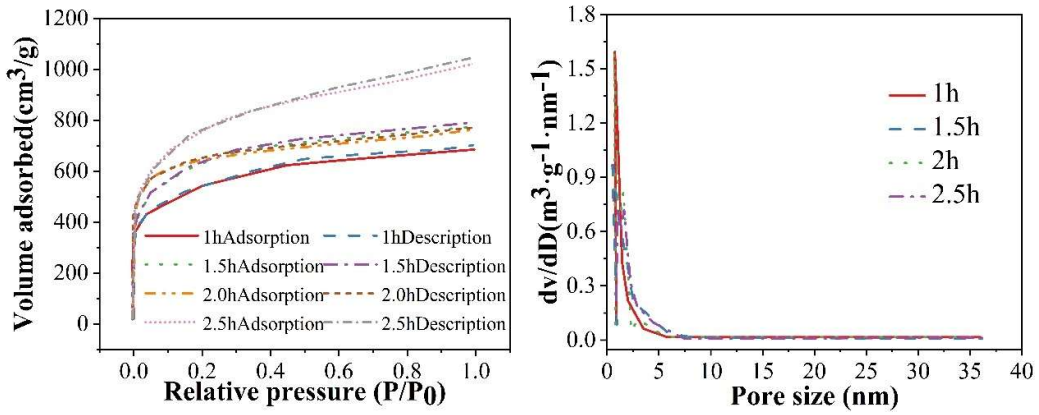

(a)Nitrogen absorption and desorption curve (b)Aperture distribution

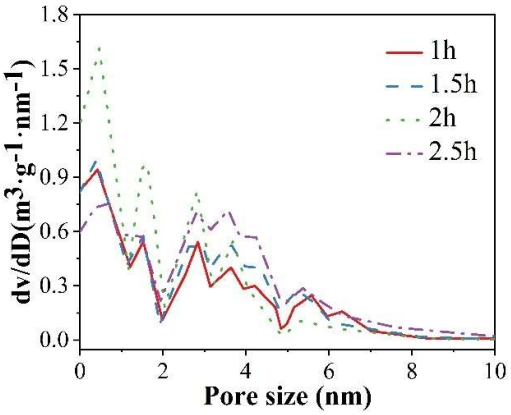

(c)0~10nmAperture distribution

Fig. 5. Study of material specific surface area and pore size distribution

Table 1. Material specific surface area and pore size distribution

Sample	SBET(m2/g)	Smicro(m2/g)	Vtotal(m3/g)	Vmicro(m3/g)
CNAC-1h	1826.18	1826.18	0.909	0.919
CNAC-1.5h	2226.17	2226.17	1.209	1.209
CNAC-2.0h	2429.08	2429.08	1.374	1.374
CNAC-2.5h	2713.31	2446.16	1.549	1.136

4.2. Effect of bitumen pretreatment on the electrochemical properties of porous carbon

As can be seen from the above analysis, the effect of asphalt pretreatment on the structure of porous charcoal was understood, mainly in XRD characterization, Raman spectroscopy, material ratio, pore size distribution, and XPS. Also with the help of finite element analysis software, the effect of asphalt pretreatment on the electrochemical properties of porous carbon is investigated from three dimensions: constant current charge/discharge, cyclic voltammetry, and AC impedance. The specific analysis process in this subsection is as follows:

4.2.1. Constant current charge/discharge test. With the support of finite element software, the effect of air oxygen method on the constant current charge and discharge performance of porous carbon samples was explored, and the constant current charge and discharge test results are shown in Figure 6, in which (a)~(b) are 0.1A•g^{-1} and 0.1~10A•g^{-1}, respectively. The GCD curves of the porous carbon samples at 0.1 A•g^{-1} are similar to the "isosceles triangle", especially the CNAC-1h, CNAC-2.0h and CNAC-2.5h have no "ohmic drop", and the triangular curves are slightly "expanded", indicating that the charge and discharge reversibility is strong, and it has a certain pseudocapacitance. Under the action of air oxygen method, the charging and discharging time of CNAC-1.5h is the longest, indicating that its specific capacitance is the highest, but there is a certain degree of tailing, which is caused by its relatively small aperture. Fig. 6(b) shows the specific capacitance of porous carbon at 0.1~10 A•g^{-1}, and at 0.1A•g^{-1}, the order of specific capacitance is: CNAC-1.5h> CNAC-2.0h> CNAC-2.5h> CNAC-1.0h, in the same order as its specific surface area size, is because the micropores in the porous carbon can be slowly and fully filled by ions in the electrolyte after asphalt pretreatment during low-current charging and discharging, and the specific surface area is the main factor affecting the specific capacitance. When the current density is large, due to the reason of same-sex repulsion, the electrolyte ions cannot fully enter the micropores, occupy all the active points, and form a large area of electric double layer, so with the gradual increase of the current density, the specific capacitance of the porous carbon decreases. Among them, the smallest decline rate is CNAC-2.0h, the specific capacitance is 129F•g^{-1} at 0.1A•g^{-1}, and the specific capacitance is 100F•g^{-1} at 10A•g^{-1}, that is, the charge-discharge

rate increases to 19.89 times of the original, and the specific capacity remains 71.92% when the specific capacity is 0.1A•g^{-1}. Mesopores provide a fast channel for charge transmission, so that the charge can smoothly enter the active point in the micropores, and the macropores act as a "buffer warehouse", which shortens the distance between the mesopores and the microholes, resulting in a high specific capacitance at high charge-discharge rates.

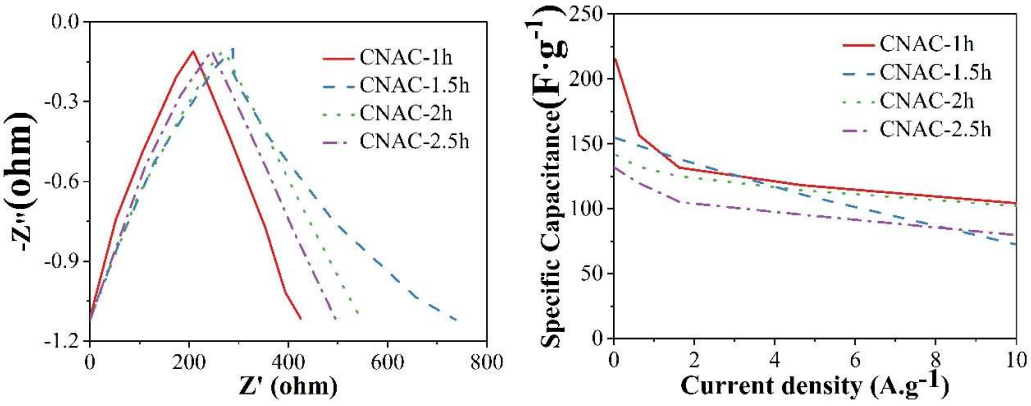

(a)0.1A·g-1 (b)0.1~10A·g-1

Fig. 6. Constant current charge and discharge test

4.2.2. Cyclic Voltammetry. With the help of finite element software, the effect of air oxygen method on the cyclic voltammetry performance of porous carbon samples was explored, and the results of cyclic voltammetry are shown in Figure 7. It can be seen from Fig. 7(a) that the CV curves of CNAC-1h, CNAC-1.5h, CNAC-2.0h, and CNAC-2.5h at 1mv•s^{-1} are approximately rectangular, and the enclosed area is relatively large, and there is an upward protruding "hump" between -1.013--0.13V, indicating that the large specific capacitance of these four samples mainly comes from the electric double layer capacitance, and the pseudocapacitance introduced by the heteroatom functional groups on the surface also makes a certain contribution. However, the CV curves of PC0 and CNAC-1h resemble elongated and deformed rectangles, and the enclosed area is small, indicating that their specific capacitance is small, which is caused by their small specific surface area. Fig. (7)b shows the CV curves of CNAC-2.5h at 10~200my-s-1, and it can be seen that the four curves are approximately rectangular, indicating that its rate performance is good, and even under the action of asphalt pretreatment, the porous carbon still maintains the pseudocapacitance "hump" characteristic, showing that the stability of its surface functional groups is good.

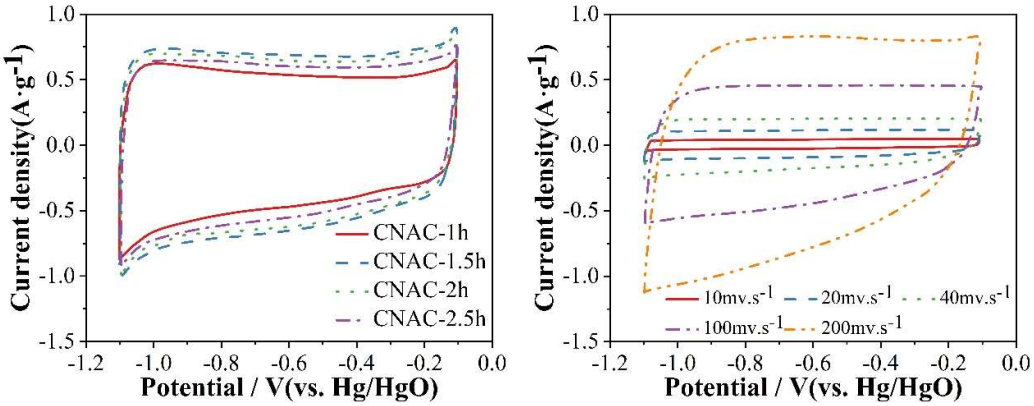

(a)5 mv.s-1CV curve of porous carbon (b)5~100 mv·s-1CV curve

Fig. 7. Cyclic voltammetry test

4.2.3. AC impedance testing. The finite element analysis software was used to investigate the effect of air-oxygen method in asphalt treatment on the AC impedance performance of porous charcoal, and the AC impedance test results are shown in Fig. 8. As can be seen from Fig. (8)a, in the low frequency region, the angle between the extension line of the AC impedance curves and the Z' axis is close to 90° for all four samples, which shows good capacitive performance. As can be seen from Fig. (8)b, in the mid-frequency region, the arc span of the EIS curve of CNAC-2h is the smallest, indicating that the electrolyte ions have less transmission and diffusion resistance inside its pores. In the high-frequency region, the intersection values of the EIS curves of the porous carbon samples with the Z' axis are all less than 0.588 Ω, indicating that the equivalent resistance of the dual-ionic liquid-based porous carbon is smaller and more conductive. The reason for this phenomenon is that after the asphalt treatment (air-oxygen method), which makes CNAC-2h have a higher specific surface area and a multilevel pore distribution of micro-, meso-, and macropores, the diffusion, transport, and adsorption of electric charge in its interior, is more smooth and rapid. The higher graphitization degree caused by the higher carbonization temperature and the introduction of phosphorus resulted in the higher electrical conductivity and lower electrical resistance of the nitrogen, phosphorus, and sulfur co-doped porous carbon.

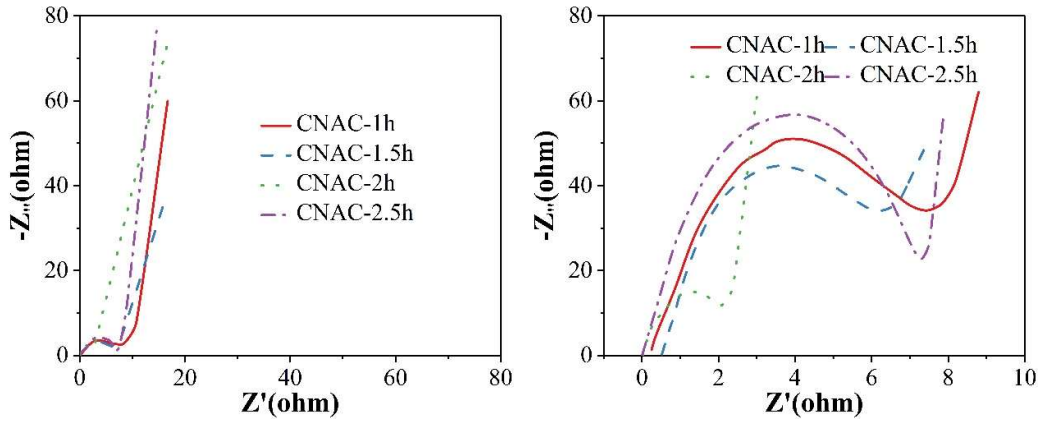

(a)Full spectrum diagram (b)High and medium frequency areas

Fig. 8. Ac impedance spectrum of porous carbon

5. Conclusion

In this paper, the porous carbon samples for this study were prepared under the guidance of the relevant preparation process. In order to reveal the effect of asphalt pretreatment on the structural and electrochemical properties of porous carbon, a relevant research program was developed and explored and analyzed with the help of finite multivariate analysis software. As the oxidation time increased to 2.5 h, the number of micropores below 0.9 nm decreased, but the micropores above 0.9 nm showed an increasing trend, while the specific surface area of porous carbon also increased with the oxidation time. In addition, the longest charging and discharging time of CNAC-1.5h was observed for the porous carbon samples after asphalt pretreatment, indicating that the constant-current charging and discharging performance of the porous carbon samples was significantly improved after the influence of the air-oxygen method for 1.5 h. The other cyclic voltammetry and AC impedance are based on the data in the paper. This paper better demonstrates the effect of asphalt pretreatment on the structural and electrochemical properties of porous charcoal, which is of great guiding value for the development of the field of materials chemistry.

References

[1] Filonchyk, M., Peterson, M. P., Zhang, L., Hurynovich, V., & He, Y. (2024). Greenhouse gases emissions and global climate change: Examining the influence of CO2, CH4, and N2O. Science of The Total Environment, 173359.

[2] Yuan, X., Su, C. W., Umar, M., Shao, X., & LobonŢ, O. R. (2022). The race to zero emissions: Can renewable energy be the path to carbon neutrality?. Journal of Environmental Management, 308, 114648.

[3] Ragupathy, P., Bhat, S. D., & Kalaiselvi, N. (2023). Electrochemical energy storage and conversion: An overview. Wiley Interdisciplinary Reviews: Energy and Environment, 12(2), e464.

[4] Pomerantseva, E. (2022). Chemical preintercalation synthesis of versatile electrode materials for electrochemical energy storage. Accounts of chemical research, 56(1), 13-24.

[5] Chakraborty, R., Vilya, K., Pradhan, M., & Nayak, A. K. (2022). Recent advancement of biomass-derived porous carbon based materials for energy and environmental remediation applications. Journal of Materials Chemistry A, 10(13), 6965-7005.

[6] Jia, Z., Zhang, X., Gu, Z., & Wu, G. (2023). MOF-derived Ni-Co bimetal/porous carbon composites as electromagnetic wave absorber. Advanced Composites and Hybrid Materials, 6(1), 28.

[7] Raji, A., Nesakumar, J. I. E. T., Mani, S., Perumal, S., Rajangam, V., Thirunavukkarasu, S., & Lee, Y. R. (2021). Biowaste-originated heteroatom-doped porous carbonaceous material for electrochemical energy storage application. Journal of Industrial and Engineering Chemistry, 98, 308-317.

[8] Nanzumani, N. M., Agyemang, F. O., Mensah-Darkwa, K., Appiah, E. S., Arthur, E. K., Gikunoo, E., ... & Raji, A. (2022). Molten salt synthesis of nitrogen-doped hierarchical porous carbon from plantain peels for high-performance supercapacitor. Journal of Electroanalytical Chemistry, 920, 116645.

[9] Di, X., Wang, Y., Lu, Z., Cheng, R., Yang, L., & Wu, X. (2021). Heterostructure design of Ni/C/porous carbon nanosheet composite for enhancing the electromagnetic wave absorption. Carbon, 179, 566-578.

[10] Yan, B., Zheng, J., Feng, L., Zhang, Q., Zhang, C., Ding, Y., ... & He, S. (2023). Pore engineering: Structure-capacitance correlations for biomass-derived porous carbon materials. Materials & Design, 229, 111904.

[11] Jiang, G., Senthil, R. A., Sun, Y., Kumar, T. R., & Pan, J. (2022). Recent progress on porous carbon and its derivatives from plants as advanced electrode materials for supercapacitors. Journal of Power Sources, 520, 230886.

[12] Li, B., Xiong, H., & Xiao, Y. (2020). Progress on synthesis and applications of porous carbon materials. International Journal of Electrochemical Science, 15(2), 1363-1377.

[13] Tian, W., Zhang, H., Duan, X., Sun, H., Shao, G., & Wang, S. (2020). Porous carbons: structure‐oriented design and versatile applications. Advanced Functional Materials, 30(17), 1909265.

[14] Dong, D., Zhang, Y., Xiao, Y., Wang, T., Wang, J., Romero, C. E., & Pan, W. P. (2020). High performance aqueous supercapacitor based on nitrogen-doped coal-based activated carbon electrode materials. Journal of colloid and interface science, 580, 77-87.

[15] Xie, L., Su, F., Xie, L., Guo, X., Wang, Z., Kong, Q., ... & Chen, C. (2020). Effect of pore structure and doping species on charge storage mechanisms in porous carbon-based supercapacitors. Materials Chemistry Frontiers, 4(9), 2610-2634.

[16] Apostolidis, P., Liu, X., Erkens, S., & Scarpas, T. (2022). Oxidative aging of epoxy asphalt. International Journal of Pavement Engineering, 23(5), 1471-1481.

[17] Zhang, Y., Hao, J., Liu, H., Chen, C., & Shi, S. (2025). Technical development of modified emulsion asphalt: A review on the preparation, performance, and applications. Reviews on Advanced Materials Science,

64(1), 20240078.

[18] Zhang, S., Yan, Y., Yang, Y., & Ding, T. (2024). Effect of the reclaiming degree of catalytic pre-desulfurization recycled crumb rubber on the properties of modified asphalt. Case Studies in Construction Materials, 20, e03224.

[19] Gorbunova, O. V., Baklanova, O. N., Gulyaeva, T. I., Arbuzov, A. B., Trenikhin, M. V., & Lavrenov, A. V. (2022). Effect of thermal pretreatment on porous structure of asphalt-based carbon. Journal of Materials Science, 57(14), 7239-7249.

[20] Behravan, A., Lowry, M., Ashraf-Khorasani, M., Tran, T. Q., Feng, X., & Brand, A. S. (2023). Effect of pretreatment on reclaimed asphalt pavement aggregates for minimizing the impact of leachate on cement hydration. Cement and Concrete Research, 173, 107305.

[21] Zhang, J., Chen, M., Leng, B., Wu, S., Chen, D., & Zhao, Z. (2024). Investigation on storage stability, H2S emission and rheological properties of modified asphalt with different pretreated waste rubber powder. Journal of Cleaner Production, 456, 142469.

[22] Naser, M. Z., Hawileh, R. A., & Abdalla, J. (2021). Modeling strategies of finite element simulation of reinforced concrete beams strengthened with FRP: A review. Journal of Composites Science, 5(1), 19.

[23] Maxim A. Olshanskii,Arnold Reusken & Paul Schwering. (2025). A Narrow Band Finite Element Method for the Level Set Equation. SIAM Journal on Scientific Computing,47(2),A762-A789.

[24] Xiaori Wang,Zheyu Zhang,Zitao Tang,Haoyuan Yang,Jun Zou & Xiuting Zhao. (2025). Design and optimization of sliding support structure for external windows based on ANSYS. Journal of Physics: Conference Series,2954(1),012050-012050.

[25] Greice K.B. da Costa,Ada López,Sandra Pedro & Lilian Sosman. (2024). Behavior analyses of chromium into LiZnNbO4 host through optical spectroscopy and X-ray diffraction. Journal of Molecular Structure,1306,137897-.